Wiley Online Library
Early View publication on www.wileyonlinelibrary.com
(issue and page numbers not yet assigned;
citable using Digital Object Identifier – DOI)

Phys. Status Solidi C, 1–7 (2016) / DOI 10.1002/pssc.201600107

physica status solidi c
www.pss-c.com
current topics in solid state physics

High-induction nanocrystalline soft magnetic $Fe_XTi_YB_Z$ films prepared by magnetron sputtering

Elena N. Sheftel[1], Valentin A. Tedzhetov[*,1], Eugene V. Harin[1], Filipp V. Kiryukhantsev-Korneev[2], and Galina Sh. Usmanova[1]

[1] A. A. Baikov Institute of Metallurgy and Material Science, Russian Academy of Sciences, Leninsky pr. 49, 119991 Moscow, Russia
[2] National University of Science and Technology "MISIS", Leninsky pr. 4, 119049 Moscow, Russia

Received 5 July 2016, revised 30 August 2016, accepted 30 August 2016
Published online 19 September 2016

Keywords magnetron-sputtered Fe-based films, nanocrystalline structure, phase and structural states, static magnetic properties

* Corresponding author: e-mail velmurad@yandex.ru, Phone: +7 499 135 9663

To design films with the Fe/TiB_2 nanocomposite structure, which are characterized by high saturation induction B_s, the phase and structural states and static magnetic properties of Fe-TiB_2 films prepared by magnetron sputtering and subjected to subsequent annealing have been studied. According to X-ray diffraction data, either amorphous or nanocrystalline single-phase structure (an α-Fe(Ti,B) supersaturated solid solution with a bcc crystal lattice) is formed in the as-sputtered films. Depending on the film composition, the grain size of the α-Fe(Ti,B) phase varies from 45.6 to 6.5 nm; grains are characterized by high microstrain (0.21-4.96%). The annealing at 200-500 °C leads to a decrease in the lattice parameter of the α-Fe(Ti,B) phase, i.e. to its depletion of titanium and boron and to the formation of two-phase α-Fe + Fe_3B structure after annealing at 500 °C. The annealing at 200-500 °C almost does not affect the grain size and microstrain of the bcc α-Fe-based phase. The amorphous state of the films is stable up to 500 °C. All studied films are ferromagnets; the saturation induction B_s (0.95-2.13 T) and coercive field H_c (0.4-5 kA/m) of the films were determined. Correlations between the B_s and H_c magnitudes and the chemical composition of the films, their phase and structural states and magnetic structure are discussed.

1 Introduction

Principal trends of the modern development of magnetic microelectronics are the miniaturization and performance to ensure the efficient operation in magnetic fields of MHz and GHz frequencies. Therefore, the design of new magnetic materials, the properties of which allow one to implement the aforementioned tendencies, is the actual materials science problem. Revolutionary changes in magnetic microelectronics, which started in 90th of the last century, were substantially initiated by experimental data on unique magnetic properties of nanocrystalline ferromagnets [1]. This resulted in the development and application of a number of Fe-based nanocrystalline alloys prepared in the form of melt-spun ribbons 10-50 μm in thickness [2].

At the same time, research community showed an interest in a new class of soft magnetic nanocrystalline Fe-Me-X alloys (Me is one of transition metals of IV Group of the Periodic Table and X is one of light elements N, C, O, B) prepared in the form of the films [3-5]. The particular interest in such films is related to their possible application as magnetic cores of read/write heads in miniature quick-acting AV-equipment devices [6]. The physical-chemical approach used in choosing the chemical composition of new-class films and conditions for the formation of their structure was first formulated in [7], which, as was shown later by an example of Fe-Zr-N films [8], assure the combination of high saturation induction B_s, low coercive field H_c, and high hardness.

The approach consists in choosing a quasi-binary eutectic Fe-MeX alloy, preparation of the alloyed films in amorphous or cluster state by magnetron sputtering, and subsequent annealing that forms the nanocrystalline structure in the films. The nanocrystalline structure should con-

sist of the matrix ferromagnetic Fe-based phase and disperse inclusions of nonmagnetic thermodynamically stable hard interstitial MeX phase, which strengthen the matrix phase (a Fe/MeX nanocomposite structure).

The described approach was used for soft magnetic bulk Fe-based alloys prepared by casting. As a result, the alloys, in particular the Fe(9.5 wt.% Si-5.5 wt.% Al)-TiB_2 alloy, were developed. The alloys are characterized by the combination of magnetic (high saturation induction and magnetic permeability at MHz frequencies) and mechanical (hardness and wear resistance) properties that were not reached for other bulk soft magnetic alloys [9, 10].

In contrast to data on bulk soft magnetic alloys, no data on the film Fe-based alloys containing hard nonmagnetic TiB_2 phase particles are available in the literature.

In this regard, in order to study the possibility of preparation of Fe/TiB_2 nanocomposite films with the high saturation induction B_s, we investigated the phase and structural states and static magnetic properties of Fe-TiB_2 alloys prepared by magnetron sputtering and subsequently annealed.

2 Experimental

Films for the investigation were prepared by dc magnetron sputtering of a target, which consists of a Fe disc with TiB_2 ceramic chips uniformly distributed on the disc (Fig. 1). To prepare films differing in the Ti and B content, the number of TiB_2 chips was varied (Table 1).

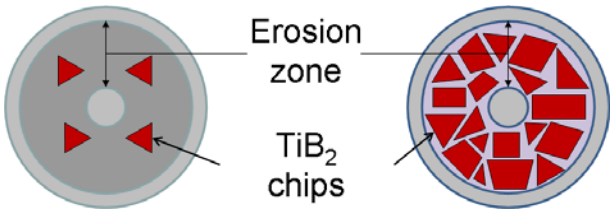

Figure 1 Scheme of the Fe-TiB_2 targets.

Table 1 Preparation conditions and chemical composition of the films under study.

No.*	S**, %	U, V	I, A	t, min	h***, μm	chemical composition, at.%
0	0	500	1.5	7	1.75	$Fe_{97.8}O_{2.2}$
I	1.9	550	1.5	5	0.4	$Fe_{97.5}Ti_{0.5}B_{0.5}O_{1.5}$
II	5.1	550	1.5	5	0.5	$Fe_{96.2}Ti_{1.0}B_{1.0}O_{1.8}$
III	8.3	600	1.5	5	0.4	$Fe_{94.4}Ti_{2.0}B_{1.9}O_{1.7}$
IV	14	500	1.5	10	0.4	$Fe_{87.1}Ti_{3.7}B_{7.2}O_{2.0}$
V	21	500	1.5	10	0.3	$Fe_{72.4}Ti_{5.4}B_{19.2}O_{3.0}$
VI	37	550	1.7	10	0.3	$Fe_{54.5}Ti_{14.3}B_{28.9}O_{2.3}$

* Film series.

** Area of TiB_2 chips on Fe target.

*** Film thickness.

The sputtering was performed in an argon atmosphere at the pressure $P_{Ar} = 0.2 \div 0.3$ Pa. Glass plates 1.5 mm thick were used as the substrates (the dielectric material is used in microelectronics as substrates for magnetic films or isolating layers in multilayer magnetic systems). Additionally, the Ni-15 wt.% Cr-8.5 wt.% alloy discs were used as the substrates. Table 1 shows preparation conditions of the studied films. The average rate of film deposition was 0.03÷0.1 μm/min. The films were annealed at 200, 300, 400 and 500 °C for 1 h at the residual pressure 2×10^{-4} Pa.

The microstructure of cross-sections of films and their chemical composition were studied by scanning electron microscopy (SEM) and energy dispersive X-ray (EDX) spectroscopy using Hitachi S3400N equipped with Noran 7 Thermo Scientific. To accurately determine the content of light elements in the films, glow-discharge optical emission spectroscopy (GDOES) [11] was used, which was performed on Horiba Jobin Yvon Profiler-2. This method was used to determine the element distribution across the thickness of film deposited on Ni alloy disc and to estimate the film thickness with accuracy ±15%.

The phase composition and fine structure of the films (coherent domain size corresponding to grain size D and Gauss root-mean square microstrain ε on grain scale) were determined by X-ray diffraction (XRD) analysis using Rigaku Ultima IV diffractometer equipped with a graphite monochromator, CuK_α radiation, and Bragg-Brentano geometry; patterns were taken for a 2θ angular range of 20-120º at a step of 0.2º. Scintillation and semiconductor detectors were used to detect reflection.

Experimental data were initially processed by Outset program [12], which was used also to calculate the lattice parameters. Qualitative phase analysis was performed using Phan program and Joint Committee on Powder Diffraction Standards Data [12]. Quantitative phase analysis and determination of the grain size and root-mean-square microstrain ε were performed using full-profile Rietveld refinement method and Phan% program [12]. XRD patterns were approximated using root-mean-square method by pseudo-Voigt function; this allowed us to calculated the centroid ($2\theta_{max}$) corresponding to reflections of phases in the studied films.

Magnetic hysteresis loops were measured in magnetic fields up to 1.27 MA/m using a LakeShore 7407 vibrating-sample magnetometer. To determine the saturation induction of material's unit volume, the magnetic moment of sample, which was measured in emu units (emu = 10000T·cm^3/4π), was divided by the film volume that was calculated using the film surface area and film thickness determined by GDOES. All measurements were performed at room temperature.

3 Results and discussion

According to chemical analysis data (Table 1), all the films contain Fe, Ti, B, and O; as the percentage of TiB_2 chips increases, the Ti and B contents increase and vary

from 0 to 14.3 and 28.9 at.%, respectively. The presence of oxygen can be explained by insufficient pump-down of vacuum chamber (the residual pressure is ~10^{-3} Pa) and the presence of impurity oxygen in the operating gas atmosphere (the purity of used argon and nitrogen gases is 99.993 and 99.999%, respectively) and in cathode raw materials as well. Taking into account the fact that the oxygen content in the films mainly does not exceed 2.5 at.% (1 wt.%), we can consider, according to data of [13], the prepared films as ternary Fe-Ti-B alloys (Fig. 2).

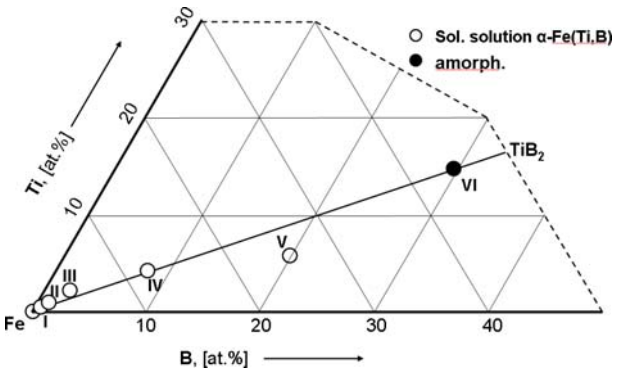

Figure 2 Chemical compositions of studied as-sputtered films in the nanocrystalline (open circles) and XRD amorphous (filled circles) states.

According to SEM data, the studied films have a dense structure and are free from pores (Fig. 3a). Element distribution profiles obtained by GDOES (Fig. 3b) show the uniform distribution of the principal components across the film thickness.

The $Fe_{97.8\text{-}72.4}Ti_{0\text{-}5.4}B_{0\text{-}19.2}O_{1.5\text{-}3.0}$ films (series 0, I-V) in the as-sputtered state have single-phase crystal structure. XRD patterns of the films (Fig. 4a) indicate peaks corresponding to 2θ = 44.7, 65.0 and 82.4°, which can be respectively identified as the (110), (200) and (121) reflections of the α-Fe-based phase with a bcc crystal lattice (from herein, bcc phase). As the Ti and B contents in the films increase, the angular positions of the reflections shift to the low-angle range; this indicates an increase in the crystal lattice parameter. The higher the Ti and B contents, the more the crystal lattice increases (Fig. 5). Taking into account the fact that the equilibrium titanium solubility in α-Fe is low (2.9 at.% at 500 °C [14]) and the fact that the B solubility is almost absent (≤0.001 at.% at 500 °C [14]), the observed increase in the lattice parameter indicates the formation of α-Fe-based solid solution that, under high-energy synthesis conditions, is supersaturated with boron and titanium. It is possible because of the high titanium affinity to oxygen, that partially or completely fixes oxygen available in the material to form either Ti(O) solid solution or one of equilibrium oxide phases in the Ti-O system [14]. The obvious high dispersion of the phase and its small amount do not allow us to detect it by XRD analysis. The as-sputtered $Fe_{54.5}Ti_{14.3}B_{28.9}O_{2.3}$ films (series VI) are amorphous.

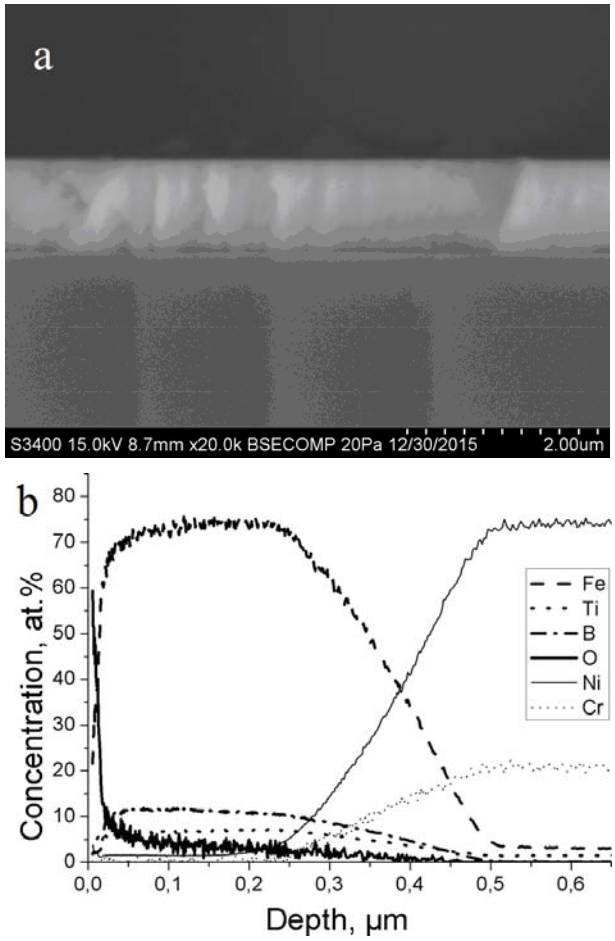

Figure 3 (a) Microstructure (SEM image) of cross section of the $Fe_{94.4}Ti_{2.0}B_{1.9}O_{1.7}$ film and (b) element distribution profile (GDOES) across the thickness of the $Fe_{72.4}Ti_{5.4}B_{19.2}O_{3.0}$ films.

The films of series 0 and I-V have the nanocrystalline structure. In this case, the bcc-phase grain size in the films containing 3.7-5.4 at.% Ti and 7.2-19.2 at% B (series IV and V) is substantially lower (5-12 nm) than 25-35 nm in the films with 0.5-2.0 at.% Ti and 0.5-1.9 at.% B (series I-III, Fig. 5). This fact confirms the formation of solid solutions and indicates hindered diffusion processes, which lead to the difficult grain growth in solid solutions with the higher alloying element concentrations.

The high microstrain in bcc-phase grains (Fig. 6), which is 0.21-0.44% for the $Fe_{97.8\text{-}87.1}Ti_{0\text{-}3.7}B_{0\text{-}7.2}O_{1.5\text{-}2.2}$ films (series 0, I-IV) and 4.96% for the $Fe_{72.4}Ti_{5.4}B_{19.2}O_{3.0}$ films (series V), attracts the attention. The physical origin of so high microstrain in the studied films calls for specific investigations.

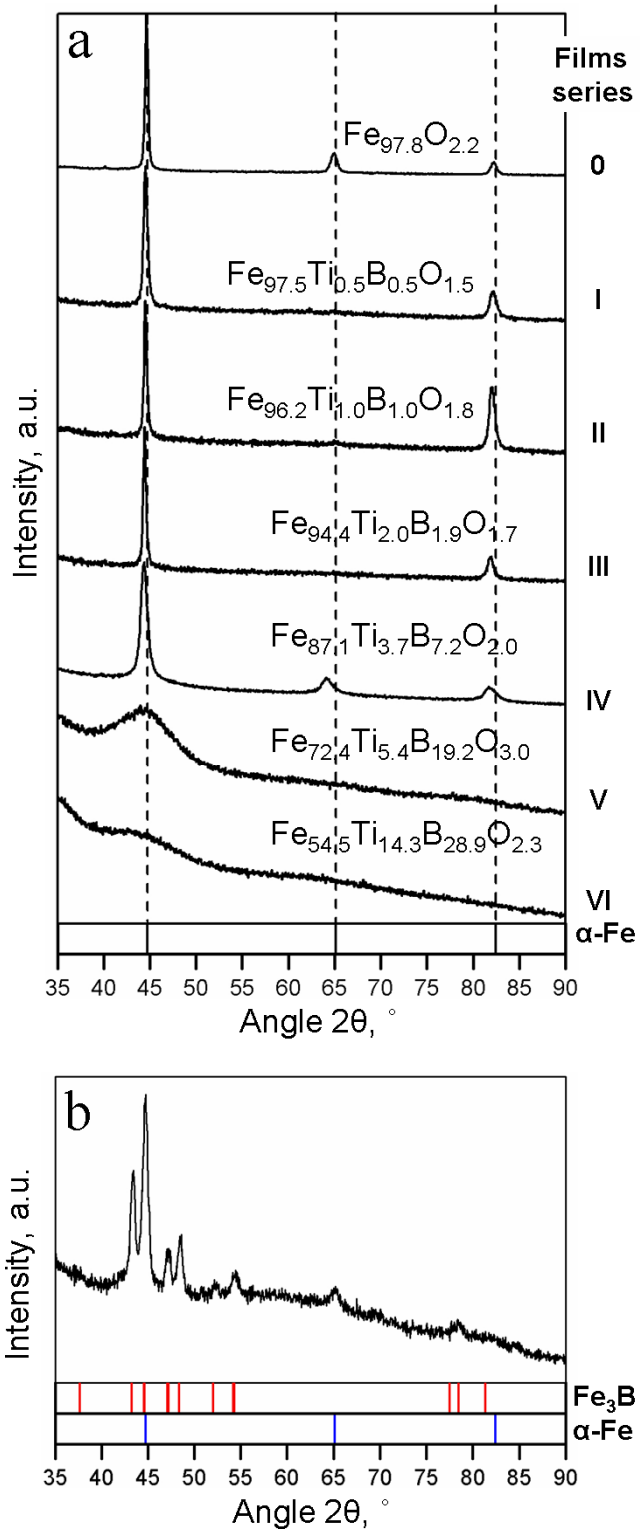

Figure 4 X-ray diffraction patterns of (a) as-sputtered films and (b) the series V film annealed at 500 °C (the blue and red bar diagrams correspond to α-Fe and Fe_3B phases, respectively).

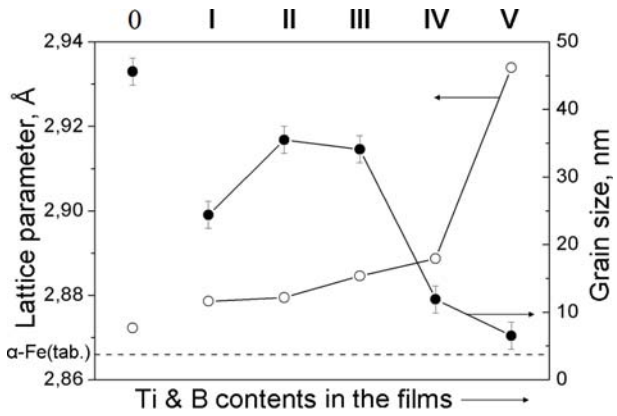

Figure 5 Lattice parameter (filled circles) and grain size (open circles) of the bcc phase as functions of the total Ti and B contents in as-sputtered films.

The annealings of the films lead to changes in XRD patterns (as compared to those for the as-sputtered state, Fig. 4b). Angular positions of bcc-phase reflections shift to the higher 2θ angles. The higher the annealing temperature is, the more substantial is the shift. This fact indicates the decrease in the lattice parameter of the bcc phase. Thus, as the annealing temperature increases, alloying elements leave the solid solution, and the lattice parameter of the bcc phase approaches to pure α-Fe (2.866 Å, Fig. 6a). The fact that the lattice parameter (2.857 Å) of the $Fe_{72.4}Ti_{5.4}B_{19.2}O_{3.0}$ film (series V) annealed at 400 and 500 ºC is lower than that of α-Fe (Fig. 6a) attracts the attention. Differences between the lattice parameters of metals and alloys with nanocrystalline and microcrystalline structures were discussed in a number of works [15, 16]. The annealing of the $Fe_{72.4}Ti_{5.4}B_{19.2}O_{3.0}$ films (series V) at 500 ºC leads to the formation of the two-phase α-Fe + Fe_3B structure; the volume ratio of the phases is 4:1, respectively (Fig. 4b). According to the equilibrium phase diagrams [13, 14], the composition of the series V films (Fig. 2) should correspond to the three-phase α-Fe + Fe_3B + Ti_2B region. The absence of the Ti_2B phase in films of series V indicates the fact that, when the phase composition forms, kinetics factors prevail over thermodynamic factors. Indeed, despite of the fact that the enthalpy of formation of the Ti_2B compound ($-\Delta H^f$ = 324 kJ/mol) is substantially higher than it of the Fe_3B compound ($-\Delta H^f$ = 18 kJ/mol), the later compound forms because its components are present in the films in greater amount (law of mass action).

The annealing of series I-IV films at all temperatures under study almost does not affect the grain size of the bcc phase and its microstrain; in this case, the differences between the grain size and microstrain of the films with low Ti and B contents (series I-III) and those of the films with high Ti and B contents (series IV, V) remain (Figs. 6b, c). The absence of grain growth and remained sufficiently high microstrain allow us to assume that boron atoms leaving the solid solution during annealing are used to form the

Fe_3B phase; the structure becomes two-phase (bcc α-Fe-based phase + Fe_3B). One of the lattice parameters of the Fe_3B tetragonal lattice (a = 8.625 Å) is almost equal to the threefold lattice parameter of α-Fe; this creates conditions for the lattice coherency of these phases. In this case, the formed Fe_3B particles, despite of their high dispersion and insignificant amount (XRD analysis does not reveal the phase), suppress the bcc-phase grain growth and remain the high microstrain during annealing. It is possible also that boron atoms leaving the solid solution partially "deposite" at bcc-phase grain boundaries (since boron is the surface active element [17, 18]) and prevent the bcc phase grain growth.

Titanium partially was present in the solid solution and leaves it during annealing. Subsequently titanium forms one of oxygen-containing Ti-O phase, which, as was mentioned above, begins to form already during deposition of the films [19].

The aforementioned assumptions on the annealing-induced formation of two-phase structure in the series I-IV films, which consists of the matrix bcc α-Fe-based solid solution and the coherent high-dispersed Fe_3B precipitates, agree adequately with XRD data for the series V films annealed at 500 °C. According to XRD data, the two-phase α-Fe + Fe_3B structure is formed in these films; the grain size of the Fe_3B phase and its amount are sufficient to identify the phase by XRD (Fig. 4b). In this case, the lattice coherency is likely to be violated. This fact explains the substantial decrease in the microstrain ε from 4.992% for the as-sputtered film to 0.305% for the film annealed at 500°C. Among the films under study, the minimum lattice parameter (2.857 Å) of the bcc phase in these films annealed at 400 and 500 ºC (Fig. 6) indicates the fact that α-Fe, rather than the α-Fe-based solid solution, is the matrix phase in these films.

The amorphous state formed in the $Fe_{54.5}Ti_{14.3}B_{28.9}O_{2.3}$ films (series VI) with the highest Ti and B content was found to be stable up to 500°C.

All the films under study are ferromagnets. The saturation induction B_s of as-sputtered series I-V films, which, according to XRD data, are single-phase nanocrystalline (bcc α-Fe-based solid solution), varies from 0.95 to 1.8 T and increases as the Ti and B contents in the films increase (Fig. 7a). According to data of [20], the presence of boron in the α-Fe-based solid solution decreases its saturation induction B_s. This is explained by the fact [20] that in the case of boron being present in the solid solution, boron electrons fill 3d bands of Fe atoms, decrease the number of unpaired spins and, therefore, boron leads to a decrease in B_s. The observed increase in B_s of the series I-V films (Fig. 7a) should be related to the fact that, these films in the as-sputtered state are characterized by the presence of another ferromagnetic phase (along with the ferromagnetic α-Fe-based solid solution), the saturation induction of which exceeds that of the α-Fe-based solid solution. Among the possible phases formed in the studied films, the Fe_3B phase with B_s = 1.6 T [21] can be the cause for the increase in B_s. The low volume fraction and high dispersion of the phase do not allow us to find the phase by XRD. However, the observed increase in B_s of the films with increasing B content (Fig. 7a) makes the assumption reasonable.

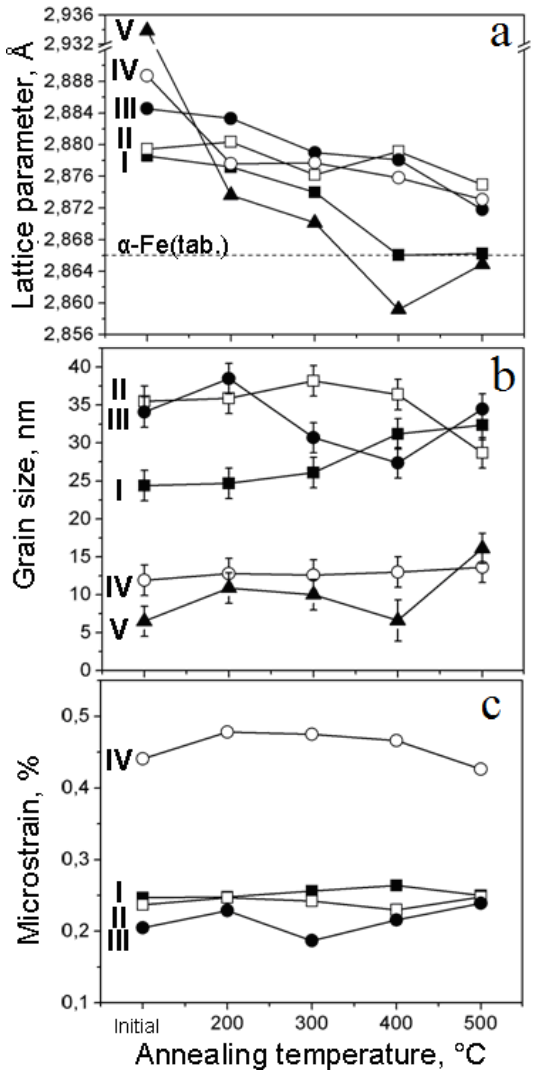

Figure 6 Effect of annealing on (a) the lattice parameter, (b) grain size, and (c) microstrain of the bcc α-Fe-based phase.

For all films under study, the annealing at 200 °C leads to the increase in the saturation induction to 1.9-2.1 T (Fig. 7a). This is explained by the fact that B and Ti atoms leave the solid solution (the lattice parameter of the α-Fe-based phase decreases, Fig. 6a); in this case, the amount of the ferromagnetic Fe_3B phase increases. This is confirmed by the identification of the phase in the series V films annealed at 500 °C (Fig. 4b). The further increase in the annealing temperature almost does not affect or weakly affects the B_s magnitude. Variations of the B_s magnitude in range of 1.9-2.1 T, which are observed in Fig. 7a after annealings higher 200 °C, are related to the fact that the sput-

tering flow from magnetron is nonuniform relatively to the target erosion zone; this leads to variations in the film thickness. As was mentioned above, the film thickness magnitude is used to determine the saturation induction magnitude. As a result, the measurement error of the saturation induction is ±15%.

The coercive field H_c magnitudes of all studied as-sputtered and annealed films remain corresponding to soft magnetic materials (Fig. 7b). As is seen from Fig. 7b data compared to Fig. 6, the H_c magnitude depends, according to a random anisotropy model [22], on the ratio of magnitudes, namely, grain size and grain microstrain, which determine the magnetocrystalline and magnetoelastic anisotropy, respectively. The increase in the H_c magnitude with the annealing temperature increase (Fig. 7b) is explained by the presence of, at least, two phases (such as the α-Fe-based solid solution and Fe_3B) having different saturation inductions and by the appearance, in this regard, of additional magnetostatic anisotropy [23].

The $Fe_{54.5}Ti_{14.3}B_{28.9}O_{2.3}$ films (series VI) are amorphous (in terms of X-ray diffraction) in both as-sputtered and annealed at all studied temperatures states. These films are weak ferromagnets, the saturation induction of which varies from 0.08 to 0.15 T depending on the annealing temperature.

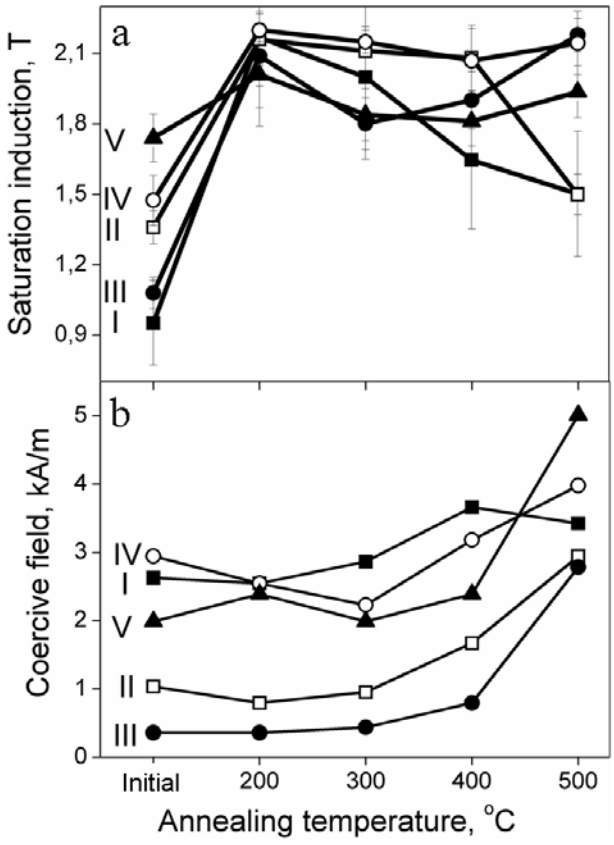

Figure 7 (a) Saturation induction and (b) coercive field of the films as functions of the annealing temperature.

4 Conclusions

1. The $Fe_{97.8\text{-}54.5}Ti_{0\text{-}14.3}B_{0\text{-}28.9}O_{1.5\text{-}3.0}$ films prepared by magnetron sputtering were subjected to 1 h annealing at temperatures of 200-500 °C.

2. According to XRD data, the as-sputtered $Fe_{97.8\text{-}72.4}Ti_{0\text{-}5.4}B_{0\text{-}19.2}O_{1.5\text{-}3.0}$ films have the single phase crystal structure, which consists of the α-Fe-based solid solution that have a bcc crystal structure and is supersaturated with Ti and/or B and presumably of high dispersion Ti-O phases. The bcc α-Fe-based phase grain size decreases from 45.6 to 6.5 nm with increasing Ti and B contents in the films. The $Fe_{54.5}Ti_{14.3}B_{28.9}O_{2.3}$ films are amorphous.

3. The as-sputtered films are characterized by high microstrain ε of bcc-phase grains, which is 0.21-0.44% for the $Fe_{97.8\text{-}87.1}Ti_{0\text{-}3.7}B_{0\text{-}7.2}O_{1.5\text{-}2.2}$ films and increases to 4.96% for the $Fe_{72.4}Ti_{5.4}B_{19.2}O_{3.0}$ films.

4. Annealing at temperatures of 200-500 °C leads to depletion of the bcc solid solution of titanium and boron (the decrease in the bcc α-Fe-based phase lattice parameter); after annealing at 500°C the two-phase α-Fe + Fe_3B structure is formed in the $Fe_{72.4}Ti_{5.4}B_{19.2}O_{3.0}$ films. The annealing at all temperatures almost does not affect the grain size and microstrain of the bcc α-Fe-based phase. The amorphous state of the $Fe_{54.5}Ti_{14.3}B_{28.9}O_{2.3}$ films is stable up to 500 °C.

5. All the films under study are ferromagnets. The saturation induction B_s of the as-sputtered nanaocrystalline films varies from 0.95 to 1.8 T and increases with increasing Ti and B contents. This fact indicates the presence of the other ferromagnetic phase that is likely to be Fe_3B. Because of the high dispersion and small amount, the phase cannot be revealed by XRD. It is characterized by saturation induction B_s (1.6 T) which is higher than the α-Fe(Ti,B) matrix ferromagnetic phase. With respect to the as-sputtered films the annealing at 200 °C leads to the increase in the saturation induction to 1.9-2.13 T. This fact indicates the further increase in the content of the Fe_3B phase.

6. The coercive field magnitudes H_c of all studied films in the as-sputtered and annealed states correspond to soft magnetic materials and depend on the ratio of magnitudes, namely, grain size and grain microstrain, which determine the magnetocrystalline and magnetoelastic anisotropy, respectively. The increase in the H_c magnitude with the annealing temperature increase is explained by the appearance of additional magnetostatic anisotropy that is induced at the interface of α-Fe(Ti,B) and Fe_3B phases characterized by different saturation inductions.

7. The $Fe_{54.5}Ti_{14.3}B_{28.9}O_{2.3}$ films with the amorphous structure are weak ferromagnets, the saturation induction B_s varies from 0.08 to 0.15 T depending on the annealing temperature.

Acknowledgements The study was supported by the Russian Foundation for Basic Research (project no. 15-08-02831a).

References

[1] Y. Yoshizawa, S. Oguma, and K. Yamauchi, J. Appl. Phys. 64, 6044 (1988).
[2] M. E. McHenry and D. E. Laughlin, Acta Mater. **48**, 223 (2000).
[3] B. Viala, M. K. Minor, and J. A. Barnard, J. Appl. Phys. **80**, 3941 (1996).
[4] A. Chakraborty, K. R. Mountfield, G. H. Bellesis, D. N. Lambeth, and M. H. Kryder, J. Appl. Phys. **80**, 1012 (1996).
[5] K. Nago, H. Sakakima, and K. Ihara, IEEE Trans. J. Magn. Jpn. **7**, 119 (1992).
[6] M. T. Rask and L. L. Longworth, US Patent 5001589A (1991).
[7] V. K. Grigorovich, E. N. Sheftel‘ et al., Report on the contract IMET-Philips PLW-938018-D-WZ-86512 (1995).
[8] E. N. Sheftel, Inorg. Mater.: Appl. Res. **1**(1), 17 (2010).
[9] O. A. Bannykh, E. N. Sheftel, V. K. Grigorovich, R. E. Strug, A. Mkrtumov, I. R. Polyukhova, and A. V. Evdokimov, Russian patent 4775860/02, 30.09.1992 Stat. No. 36 [in Russian].
[10] V. K. Grigorovich, E. N. Sheftel', R. E. Strug, and I. R. Polyukhova, Izv. Akad. Nauk SSSR-Metally No. 6, 173 (1993).
[11] Ph. V. Kiryukhantsev-Korneev, Protect. Met. Phys. Chem. Surfaces **48**, 585 (2012).
[12] E. V. Shelekhov and T.A. Sviridova, Met. Sci. Heat Treatment **42**, 309 (2000).
[13] K. Tanaka and T. Saito, J. Phase Equilibria **20**, 207 (1999).
[14] N. P. Lyakishev (Ed.), Phase Diagrams of Binary Metallic Systems, Vol. 2 (Mashinostroenie, Moscow, 1997), pp. 586-591; Vol. 3, Book 1, pp. 724-726 (1999) [in Russian].
[15] H. Gleiter and M. Fichner, Scripta Mater. **46**, 497 (2002).
[16] M. Ya. Gamarnik and Yu. Yu. Sidorin, Phys. Status Solidi B **156**, K1 (1989).
[17] N. A. Filatova, A. P. Polushko, N. Ya. Luzhanskaya, N. P. Sleptsova, and V. M. Grushevskii, Sov. Powder Metallurg. Metal Ceram. **9**, 400 (1970).
[18] G. E. Totten (Ed.), Steel Heat Treatment: Metallurgy and Technologies, 2nd ed. (CRC Press, Boca Raton, 2006), p. 194.
[19] O. M. Zhigalina, D. N. Khmelenin, E. N. Sheftel', G. Sh. Usmanova, A. L. Vasil'ev, and A. Carlsson, Cryst. Rep. **58**, 344 (2013).
[20] N. Lenge and H. Kronmüller, Phys. Status Solidi A **95**, 621 (1986).
[21] R. Coehoorn, D.B. De Mooij, and C. De Waard, J. Magn. Magn. Mater. **80**, 101 (1989).
[22] G. Herzer, Acta Mater. **61**, 718 (2013).
[23] Y. Iwama and M.Takeuchi, Trans. Jpn. Inst. Met. **15**, 371 (1974).